J. Fluid Mech. (2010), *vol.* 651, *pp.* 27–53.
doi:10.1017/S0022112009993806

Towards the design of an optimal mixer

OLEG GUBANOV AND LUCA CORTELEZZI†

Department of Mechanical Engineering, McGill University, 817 Sherbrooke Street West, Montreal, Quebec H3A 2K6, Canada

(Received 16 April 2009; revised 30 November 2009; accepted 3 December 2009; first published online 22 March 2010)

We define as an optimal mixer a mixing device able to deliver a uniformly optimal mixing performance over a wide range of operating and initial conditions. We consider the conceptual problem of designing an optimal mixer starting from a well-known reference mixer, the sine flow. We characterize the mixing performance of the reference mixer, and show that it performs poorly and erratically over a wide range of operating conditions and is quite sensitive to the geometry of the initial concentration field. We define as a target performance the best mixing performance the reference mixer is able to achieve. In steps we modify the design of the reference mixer. First, we optimize the time sequence of the switching protocols and show that the mixing performance of the time-optimized mixer, although substantially improved with respect to the reference mixer, is still far from achieving the target performance and being insensitive to the geometry of the initial concentration field. The analysis of the performance of the time-optimized mixer brings to light the deficiency of the actuating system used, which delivers always the same amount of shear at the same locations. We modify the actuating system by allowing the stirring velocity fields to shift along their coordinate axes. A new mixer, the space-optimized mixer, is created by equipping the reference mixer with the new actuating system and optimizing the shift of the stirring velocity field at each iteration. The space-optimized mixer is able to deliver the target performance over the upper two-thirds of the operating range. In the lower one-third, the performance of the space-optimized mixer deteriorates because of the use of a periodic protocol. A optimal mixer is finally obtained using the actuating system of the space-optimized mixer and coupling the time and shift optimizations. The resulting optimal mixer is able to deliver a uniform target performance, insensitive to the geometry of the initial conditions, over the entire operating range.

1. Introduction

Mixing of two or more different fluids is a crucial step in pharmaceutical, food, polymer and biotechnological processes, to name a few. In many applications, the ones targeted in this study, it is impractical or impossible to promote turbulence to enhance mixing. Mixing in the laminar regime is generally poor because the fluid motion is dominated by viscous forces. In industrial applications, poor mixing results in severe problems such as insufficient homogenization, low product quality and excessive amount of byproducts. Furthermore, the present competitive market demands a decrease in manufacturing costs of the products obtained by laminar mixing. Therefore, the problem of designing a mixing device able to deliver the

† Email address for correspondence: crtlz@cim.mcgill.ca

required degree of homogenization in the least amount of time using the least amount of energy is of great practical importance.

The study on laminar mixing began with the pioneering work by Aref (1984), who introduced the concept of chaotic advection. Aref's work stimulated numerous studies on laminar mixing (e.g. Ottino 1989; Aref & El Naschie 1995; Alvarez *et al.* 1998; Zalc & Muzzio 1999; Aref 2002; Szalai *et al.* 2003; Gleeson 2005; Gouillart, Thiffeault & Finn 2006; Phelps & Tucker 2006; Sturman, Ottino & Wiggins 2006; Vikhansky & Cox 2007). It has been shown that the quality of mixing strongly depends on the time sequence of the actuations used to stir the mixture, i.e. on the stirring protocol of the mixing device. With a poorly chosen stirring protocol, fluid homogenization can be achieved mainly by molecular diffusion.

The required quality of mixing often depends on the industrial application considered. Depending on the production constraints and physical properties of the fluids to be mixed, several different types of mixing devices have been designed over the years. Most of industrially relevant mixing devices can be subdivided into three main types: stirred vessels, extruders and static mixers (Paul, Atiemo-Obeng & Kresta 2004). In a stirred vessel, one or more shafts promote mixing by rotating impellers within a vessel filled with a mixture of two or more fluids. In an extruder, mixing is promoted by rotating one or more screws inside a barrel filled with the mixture of fluids. In a static mixer, a pressure gradient forces two or more fluids to flow through a pipe equipped with motionless elements devised to promote mixing. Stirred vessels and extruders are equipped with active actuating systems, while static mixers have passive actuating systems.

In general, the quality of mixing produced by a mixing device depends on the mechanical configuration of the device and its actuating system. For example, the mechanical configuration of a stirring vessel includes the diameter and height of the vessel, as well as the shape and location of the impellers. The mechanical configuration of an extruder includes the shape of the screws and the diameter of the barrel, while the configuration of a static mixer includes the diameter of the pipe, as well as the shape and location of the motionless elements.

The quality of mixing induced by a given mixing device with a fixed mechanical configuration in general depends on the conditions in which the device operates. Operating conditions are the values of the independent parameters that specify a mixing process and can be changed without a mechanical reconfiguration of the device. Operating conditions common to many mixers include parameters such as temperature, Reynolds and Péclet numbers. As many practical applications involve mixing of non-Newtonian fluids, operating conditions often include parameters that describe rheological properties of the fluids, such as the Deborah number. Furthermore, the operating conditions of a mixing device with an active actuating system include the independent parameters which characterize the action of the actuating system. Examples are the angular speed of the impellers in a stirring vessel and the angular speed of the screws in an extruder. Note that the interdependence of the parameters describing the operating conditions and mechanical configuration is application dependent. The range of operating conditions over which a given mixing device should operate effectively is referred to as the operating range of the device.

In recent years, attempts were made to find optimal mechanical configurations and operating conditions for several mixing devices. Cunha, Covas & Oliveira (1998) studied mixing in a polymer extruder. The authors used a genetic algorithm to determine the range of optimal operating conditions for which the extruder becomes highly mixing efficient. Rodrigo *et al.* (2003) determined the optimal operating

conditions for a prototype named as the eccentric helical axial mixer. Szalai & Muzzio (2003) determined the range of operating conditions of a static mixer for which the mixer is the most mixing efficient. Stremler & Cola (2006) and Stremler (2009) determined mechanical configurations and operating conditions that optimize mixing in a flow stirred by periodically pulsing two pairs of sources and sinks. Gibout, Guer & Schall (2006), using a genetic algorithm, optimized the mechanical design of a static mixer. Singh *et al.* (2008*a*) considered mixing in a rotated arc mixer, in which a static mixer is augmented with an active actuating system, and determined an optimal mechanical configuration for which the mixer is highly efficient. Singh *et al.* (2008*b*) characterized the mixing performance of several micromixers in terms of the mechanical configurations and operating conditions. All the above studies indicate that often the optimal mixing efficiency of a mixing device can be achieved only for a particular mechanical configuration and a narrow range of operating conditions. Outside of this range or for different mechanical configurations, the performance of the mixing device may deteriorate severely.

Often the quality of mixing depends also on the geometrical configuration of the mixture injected into the mixing device. Hobbs & Muzzio (1997) investigated this effect on the mixing efficiency of a Kenics static mixer. They found that the least effective injection location requires up to four additional mixing elements to achieve the same quality of mixing as for the most effective injection location. Zalc, Szalai & Muzzio (2003) studied the effect of injection location on the mixing efficiency of SMX static mixer. They found that the off-centre injection location considerably reduces the homogeneity of the mixture when compared with that obtained using the centreline injection location. Zalc *et al.* (2003) noted that although the sensitivity to injection location can be reduced by adding extra mixing elements, this may be impractical as it also increases the required pressure gradient and, consequently, the cost of operation. Recently, Thiffeault & Pavliotis (2008) applied a variational approach to determine the optimal source distributions which maximize mixing for a range of operating conditions.

The above studies indicate that currently a given mixing device is able to deliver the required mixing efficiency only within a small subrange of its operating range and only for a certain initial configuration of the mixture. Furthermore, in practical applications, both the operating conditions and the geometrical configuration of the mixture often vary with time and, consequently, the product quality generated by current industrial mixers also changes with time. Therefore, it is of great practical importance to design a mixing device able to maintain a uniform level of homogenization for time-dependent operating and initial configurations. Thus motivated, we consider, as a case study, the characterization and optimization of a conceptual mixing device which shares some of the problematics with the mixing devices currently in use. Our goal is to design an optimal mixer, a mixing device able to deliver the same optimal mixing performance over a wide range of operating and initial conditions while consuming the same amount of energy.

Poorly performing industrially relevant mixers often stir using a periodic protocol because this protocol can be realized at low cost. The poor performance is often due to the presence of islands of regular motion (Aref 2002; Finn, Cox & Byrne 2004; Paul *et al.* 2004 and references therein) which emerge around elliptic fixed points and greatly reduce mixing efficiency. In order to overcome this difficulty, Liu, Muzzio & Peskin (1994) suggested to enhance mixing by using *aperiodic* protocols, which do not induce elliptic fixed points and thus are more likely to produce mixtures free of islands of regular motion.

The work of Liu *et al.* (1994) stimulated the development of new mixing diagnostics. Because commonly used diagnostics, such as Poincaré sections and Lyapunov exponents, are inapplicable to aperiodic protocols, Liu *et al.* (1994) adopted the stretching field statistics and the spreading rate of passive tracers to measure the quality of mixing. Several other useful measures were reported in literature and summarized by Finn *et al.* (2004). Recently, Mathew, Mezić & Petzold (2005) introduced the *mix-norm*, a new indicator of mixing. This diagnostic is capable of quantifying the mixing efficiency of periodic and aperiodic protocols when applied to purely advective or advective–diffusive flows. In particular, the mix-norm can be used to evaluate mixing efficiency of a stirring protocol in the context of a given initial concentration field.

The introduction of aperiodic stirring protocols by Liu *et al.* (1994) was an important step towards enhancing the performance of a mixing device. However, the mixing efficiency of an aperiodic protocol can vary significantly over the operating range of a mixing device and when the protocol is applied to different initial configurations of the mixture (Cortelezzi, Adrover & Giona 2008; Gubanov & Cortelezzi 2009). This hinders the use of arbitrary chosen aperiodic stirring protocols in industrial applications.

The problem of deriving an optimal stirring protocol for an idealized mixing device was formulated as a control problem by D'Alessandro, Dahleh & Mezić (1999). They considered the *eggbeater flow* (Franjione & Ottino 1992), in which a fluid constrained on a two-dimensional torus is stirred by two velocity fields $\boldsymbol{v}_0$ and $\boldsymbol{v}_1$ acting orthogonally. The control problem was stated as follows: given the shapes of the stirring velocity profiles and a measure of mixing, find a stirring protocol which extremizes this measure by intelligently blinking $\boldsymbol{v}_0$ and $\boldsymbol{v}_1$. Using entropy as a measure of mixing and simple shear as velocity profiles, $\boldsymbol{v}_0(y) = [ay, 0]^*$, $\boldsymbol{v}_1(x) = [0, bx]^*$, $ab > 0$, where the superscript $*$ indicates transpose, D'Alessandro *et al.* (1999) derived a periodic protocol which maximizes entropy among all possible periodic sequences composed of the two shear flows $\boldsymbol{v}_0$ and $\boldsymbol{v}_1$.

The control approach to fluid mixing suggested by D'Alessandro *et al.* (1999) has been applied in recent studies by Mathew *et al.* (2007), Cortelezzi *et al.* (2008) and Gubanov & Cortelezzi (2009). Mathew *et al.* (2007) considered as a stirring flow the flow induced on a two-dimensional torus by a finite set of prescribed force fields modulated in time. They solved the problem of finding a sub-optimal protocol which minimizes a weighted sum of the mix-norm and the stirring action per unit mass.

Cortelezzi *et al.* (2008) considered the eggbeater model stirred by two orthogonal, sinusoidal velocity profiles $\boldsymbol{v}_0(y) = [\sin(2\pi y), 0]^*$ and $\boldsymbol{v}_1(x) = [0, \sin(2\pi x)]^*$. This model, also known as the sine flow (Liu *et al.* 1994), has been a popular playground for the investigation of laminar mixing (Liu *et al.* 1994; Pierrehumbert 1994; Antonsen *et al.* 1996; Alvarez *et al.* 1998; Muzzio *et al.* 2000; Szalai *et al.* 2003; Thiffeault, Doering & Gibbon 2004; Phelps & Tucker 2006). Cortelezzi *et al.* (2008) introduced the short time horizon procedure for the optimization of a stirring protocol. They showed that for several operating conditions, this procedure is able to generate stirring protocols which are nearly as mixing efficient as the optimal protocol.

A recent work (Gubanov & Cortelezzi 2009) assessed the sensitivity of the protocols obtained using the short time horizon optimization to the geometry of the initial concentration field. As benchmarks in this assessment, Gubanov & Cortelezzi (2009) used the periodic protocol and the recursive symmetry-breaking protocol, a deterministic aperiodic protocol introduced by Liu *et al.* (1994). Gubanov & Cortelezzi (2009) showed that optimized protocols are generally less sensitive to the geometry of the initial scalar field than the periodic and recursive symmetry-breaking

protocols. They concluded that the optimization of the stirring protocol is essential for achieving uniformly high quality of mixing for different initial configurations of the mixture.

In this study, we describe the process of characterizing and enhancing the mixing performance of a conceptual mixing device, the *reference mixer*. As a reference mixer, we choose the sine flow system. The sine flow is a simple model which is amenable to analysis at a moderate computational cost. At the same time, the sine flow is known to capture the complex behaviour of industrially relevant mixing devices such as Kenics static mixer (Hobbs, Alvarez & Muzzio 1997). Therefore, the techniques that substantially enhance the mixing performance of the sine flow could be in principle applied to more realistic and complex flows. Furthermore, the performance of the optimal mixer derived from the sine flow provides an upper bound for the enhancements that could be achieved in practice. We consider the pure advection case only, because we are targeting mixers operating at Péclet numbers $\geqslant 10^4$. At these Péclet numbers, it has been shown that optimal protocols designed for purely advective flows can be robustly transported to advective–diffusive flows of small diffusivities (Cortelezzi *et al.* 2008).

In § 2, we introduce the mathematical formulation of the sine flow, describe the solution to the purely advective problem and discuss the procedure for the computation of the mix-norm. In § 3, using the mix-norm as a measure of mixing, we define the range of operating conditions of the reference mixer and identify the operating conditions and initial configurations which result in the best performance of the reference mixer. We define this best performance value as the *target performance*. We show that the reference mixer achieves the target performance only within a narrow range of operating conditions, while outside of this range, the performance becomes poor and inconsistent. We show that this is mainly caused by the presence of persistent pockets of unmixed fluid, which are induced in part by the periodic stirring protocol and in part by the mechanical configuration of the reference mixer. The goal of this study is to explore the operating improvements and redesign of the reference mixer necessary to obtain an *optimal mixer*, a mixer which is able to deliver the target performance over the entire range of operating conditions and a wide range of initial configurations of the mixture.

In § 4, we introduce a new mixing device which has the same mechanical configuration and actuating system as the reference mixer, but stirs the mixture with the protocols generated by the short time horizon procedure (Cortelezzi *et al.* 2008). We refer to this device as the *time-optimized mixer*. We show that this mixer performs substantially better than the reference mixer but within two ranges of operating conditions. We demonstrate that this deterioration in performance is caused by the deficiency of the actuating system used, which delivers always the same amount of shear at the same location.

In § 5, we introduce a new mixing device which has the same geometry and uses the same protocols as the reference mixer, but has a redesigned actuating system, which allows the stirring velocity fields to shift along their coordinate axes. We refer to this mixing device as the *space-optimized mixer*. We show that this mixer is nearly insensitive to the geometry of the initial configuration of the mixture and is able to achieve the target performance in the medium/high range of operating conditions.

Finally, in § 6, an optimal mixer is obtained using the actuating system of the space-optimized mixer and coupling the time and shift optimizations. We show that the resulting mixer is able to achieve the target performance over the entire operating range and for a large set of initial configurations of the mixture. We summarize our work and draw conclusions in § 7.

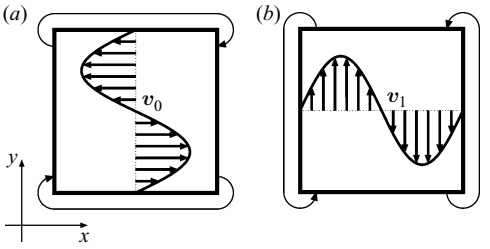

FIGURE 1. The schematic of the reference mixer. (*a*,*b*) The stirring velocity fields $\boldsymbol{v}_0$ and $\boldsymbol{v}_1$, respectively, defined in (2.1). The curves joining the opposite sides of the square mixing domain indicate periodic boundary conditions.

2. The reference mixer: the time-periodic sine flow

In this section, we introduce the time-periodic sine flow, our reference mixer. We review the solution of the purely advective problem. We also summarize the computation of the mix-norm, a measure of mixedness which is used throughout this study to assess the performance of the mixing devices and as the cost function for the optimization procedures.

2.1. *Mathematical model and operating conditions of the reference mixer*

We adopt the sine flow (Liu *et al.* 1994) as a reference mixer to develop and test our optimization and design strategies. In the sine flow model, a passive scalar field (e.g. concentration field) is stirred iteratively by a pair of orthogonal, sinusoidal velocity fields

$$\boldsymbol{v}_0(x, y) = [\sin(2\pi y), 0]^*, \quad \boldsymbol{v}_1(x, y) = [0, \sin(2\pi x)]^*, \tag{2.1}$$

inside a unit square domain with periodic boundaries; see figure 1. During each iteration, the concentration field is advected by one of the two velocity fields, $\boldsymbol{v}_0$ or $\boldsymbol{v}_1$, over a switching time τ; see figure 1. A *stirring protocol* is defined as a sequence of N binary digits $\{\alpha_k\}_{k=1}^{N}$, where N is the total number of iterations to be performed. Entries α_k set to zero and one identify the velocity fields $\boldsymbol{v}_0$ and $\boldsymbol{v}_1$, respectively. The set of 2^N binary strings of length N represents all admissible protocols that can be used to stir the mixture by a given final time $T_f = \tau N$. The sine flow stirred by the periodic protocol $\{0, 1, 0, 1, \ldots\}$ is referred to as the time-periodic sine flow and has been extensively studied (Liu *et al.* 1994; Pierrehumbert 1994; Antonsen *et al.* 1996; Alvarez *et al.* 1998; Muzzio *et al.* 2000; Adrover, Cerbelli & Giona 2002; Giona, Cerbelli & Adrover 2002; Szalai *et al.* 2003; Giona *et al.* 2004; Thiffeault *et al.* 2004; Florek & Tucker 2005; Phelps & Tucker 2006; Shaw, Thiffeault & Doering 2007; Vikhansky & Cox 2007).

The operating conditions of the sine flow are defined by the value of the switching time τ and the energy consumption. The latter, also known as the power input per unit mass, can be defined as the rate at which the actuating system does work on the mixture, and can be computed as

$$P_{in} = \frac{\mathrm{d}}{\mathrm{d}t} \int_V \frac{1}{2} \boldsymbol{v} \cdot \boldsymbol{v} \, \mathrm{d}V + \frac{1}{\rho} \int_V \boldsymbol{\sigma} : \boldsymbol{D} \, \mathrm{d}V, \tag{2.2}$$

where V is the flow domain, ρ is the fluid density, $\boldsymbol{\sigma}$ is the stress tensor and $\boldsymbol{D} = [\nabla \boldsymbol{v} + (\nabla \boldsymbol{v})^*]/2$ is the stretching tensor (Malvern 1969). Equation (2.2) states that

the power input contributes to the kinetic and internal energy of the fluids. In this study, we consider incompressible Newtonian fluids, for which the power input of the velocity fields (2.1) is $P_{in}(\boldsymbol{v_0}) = P_{in}(\boldsymbol{v_1}) = 2\pi^2\nu$, where ν is the kinematic fluid viscosity. Note that for Newtonian fluids the power input is proportional to the square of the L^2 norm of the shear rate. Owing to the above definition, restricting the energy consumption restricts the amount of shear. Throughout this study, we will derive and compare only mixing devices which perform the same amount of work and induce the same amount of shear. This allows a fair comparison of the performance of the different mixers introduced. Note that a different definition of energy consumption would not impact the results presented in the subsequent sections.

2.2. *Solution to the purely advective sine flow problem*

Pure advection of a concentration field $\varphi(x, y, t)$ is governed by the equation

$$\frac{\partial \varphi}{\partial t} = -\boldsymbol{v}_{\alpha_k} \cdot \nabla \varphi, \tag{2.3}$$

where $k = 1, 2, \ldots, N$, the iteration number, controls the time evolution of the system, i.e. $(k-1)\tau \leqslant t < k\tau$, and the velocity field $\boldsymbol{v}_{\alpha_k}$ is either $\boldsymbol{v}_0$ if α_k is zero (see figure 1*a*), or $\boldsymbol{v}_1$ if α_k is one (see figure 1*b*). We non-dimensionalize (2.3) using as characteristic time the advection time of the system, defined as $T_A = L/U$, where U is the maximum absolute value of the stirring velocity field, and L is the side of the square domain. In the sine flow system, $U = L = 1$, and $T_A = 1$. Consequently, the dimensional and dimensionless forms of (2.3) are identical.

Equation (2.3) states that in the absence of diffusion the concentration associated with any fluid particle is preserved in time. Hence, the time evolution of the concentration field can be obtained from the time evolution of fluid particles moving under the action of the stirring velocity fields (2.1).

To compute the concentration field, the unit square domain is discretized into $M \times M$ non-overlapping equal square cells, where M, the *grid resolution*, is an integer number. The concentration within the (i, j)th cell is approximated by the concentration of the fluid particle $(X^{i,j}(t), Y^{i,j}(t))$ located at time $t = t_k$ in the centre of the cell. The position of this particle is tracked backwards in time to the initial position $(X_0^{i,j}, Y_0^{i,j})$ using the map (Cortelezzi *et al.* 2008)

$$\begin{pmatrix} X_{m-1}^{i,j} \\ Y_{m-1}^{i,j} \end{pmatrix} = \begin{cases} \begin{pmatrix} X_m^{i,j} - \tau \sin(2\pi Y_m^{i,j}) \\ Y_m^{i,j} \end{pmatrix} \mod 1, & \text{if} \quad \alpha_m = 0, \\ \\ \begin{pmatrix} X_m^{i,j} \\ Y_m^{i,j} - \tau \sin(2\pi X_m^{i,j}) \end{pmatrix} \mod 1, & \text{if} \quad \alpha_m = 1, \end{cases} \tag{2.4}$$

for $m = k, k-1, k-2, \ldots, 1$. Then, the concentration associated with the (i, j)th particle at time t_k is obtained by determining its initial concentration, i.e.

$$\varphi\left(X_k^{i,j}, Y_k^{i,j}, t_k\right) = \varphi\left(X_0^{i,j}, Y_0^{i,j}, 0\right). \tag{2.5}$$

2.3. *Computation of the mix-norm*

In this study, we evaluate the performance of the reference and optimized mixing devices using the mix-norm. The mix-norm is also used as a cost function by the

optimization procedures that generate stirring protocols for the optimized mixing devices. Consequently, it is important to compute the mix-norm efficiently and accurately.

The mix-norm is a multi-scale measure of mixedness of a concentration field. It was introduced by Mathew *et al.* (2005) and is defined as the root mean square of the average values of the concentration field over a dense set of subsets contained in the flow domain. In the case of a square domain with periodic boundaries, the mix-norm μ_φ of a concentration field $\varphi(x, y, t)$ having zero mean can be computed as follows (Mathew *et al.* 2005):

$$\mu_\varphi = \sqrt{\sum_{m,n\in\mathbb{Z}} \frac{|\Phi_{m,n}|^2}{\sqrt{1+4\pi^2(m^2+n^2)}}}, \tag{2.6}$$

where $\{\Phi_{m,n}\}_{m,n\in\mathbb{Z}}$ is the spectral representation of the concentration field. Note that (2.6) is valid only for concentration fields with zero mean value. In the case when the mean concentration is not zero, the mean value must be subtracted from the concentration field before computing its spectral representation.

An approximate spectral representation of the concentration field $\varphi(x, y, t)$ can be obtained by computing the fast Fourier transform (FFT) of its discrete representation $\varphi(X_k^{i,j}, Y_k^{i,j})$, where $i, j = 1, \ldots, M$. The mix-norm is then obtained by substituting the Fourier coefficients $\Phi_{m,n}$ into (2.6). To ensure that the value of the mix-norm computed in the purely advective case is sufficiently accurate and, at the same time, the computation is feasible, in this study we use the grid resolution $M = 2048$. Gubanov & Cortelezzi (2009) discuss the details regarding this choice of the resolution. The validity of this choice is further discussed in § 3.

3. Performance of the reference mixer

In this section, we characterize the performance of the reference mixer by computing the value of the mix-norm of the concentration field at a final time T_f for a range of operating conditions, i.e. for switching time values $[\tau_{min}, \tau_{max}]$. This characterization will provide a benchmark for the optimized mixers derived in the subsequent sections.

To make our study physically meaningful, we base our choice of T_f, τ_{min} and τ_{max} on the estimates of the stretching efficiency, striation thickness and rate of folding induced by the reference mixer. Accurate computations of stretching and striation thickness induced by the sine flow for a few values of the switching time τ are available in the literature (Alvarez *et al.* 1998; Muzzio *et al.* 2000; Cerbelli, Alvarez & Muzzio 2002). However, these results are not sufficient to justify the choice of the range of switching times and T_f. To this end, we derive analytically more straightforward estimates of the stretching efficiency, striation thickness and rate of folding. We approximate the stirring induced by the velocity fields $\boldsymbol{v}_0 = [\sin(2\pi y), 0]^*$ and $\boldsymbol{v}_1 = [0, \sin(2\pi x)]^*$ near the centre of the square domain with the velocity fields $\tilde{\boldsymbol{v}}_0 = [2\pi y, 0]^*$ and $\tilde{\boldsymbol{v}}_1 = [0, 2\pi x]^*$. In this small region the shear rate $\dot{\gamma}$ of the sine flow reaches its maximum value, i.e. $\dot{\gamma} = 2\pi$. Hence, the estimates provide a bound for the stretching efficiency, striation thickness and rate of folding of the sine flow.

The dimensionless stretching efficiency e_λ of the reference mixer is (Ottino 1989)

$$e_\lambda = \frac{\mathrm{d}\ln\lambda/\mathrm{d}t}{\sqrt{\boldsymbol{D}:\boldsymbol{D}}}, \tag{3.1}$$

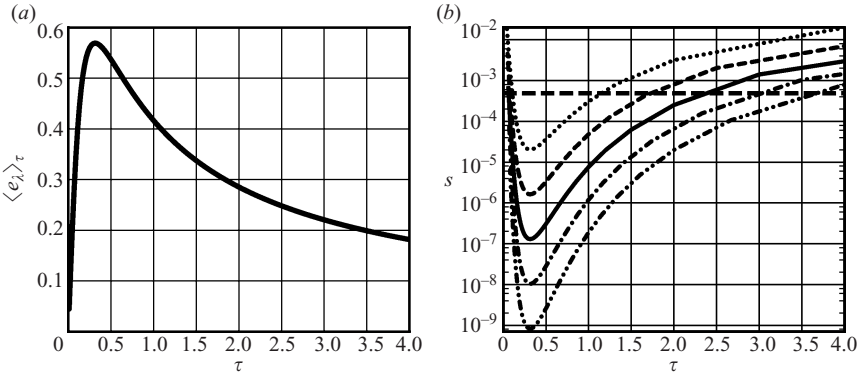

FIGURE 2. (*a*) The estimate of the stretching efficiency $\langle e_\lambda \rangle_\tau$ of the reference mixer as a function of the switching time τ. (*b*) Estimates of the final striation thickness induced by the final times $T_f = 4$ (dotted line), $T_f = 5$ (dashed line), $T_f = 6$ (solid line), $T_f = 7$ (dash-dotted line) and $T_f = 8$ (dash-dot-dotted line) as a function of the switching time τ. The horizontal dashed line indicates the value of striation thickness equal to the side of one pixel at resolution $M = 2048$.

where $\mathrm{d}\ln\lambda/\mathrm{d}t$ is the rate of stretching. For a simple shear flow the shear rate is $\dot{\gamma} = \sqrt{2\boldsymbol{D} : \boldsymbol{D}}$ and the stretching of a fluid element initially aligned, for example, with y axis is $\lambda(t) = [(\dot{\gamma}t)^2 + 1]^{1/2}$. Substituting the estimate for λ into (3.1) and averaging over the time interval $[0, \tau]$, we obtain

$$\langle e_\lambda \rangle_\tau = \frac{\ln[(\dot{\gamma}\tau)^2 + 1]}{\dot{\gamma}\tau\sqrt{2}}. \tag{3.2}$$

The stretching efficiency estimated by (3.2) is shown in figure 2(*a*). It reaches its maximum value at $\tau = 1/\pi \approx 0.315$.

The striation thickness $s(t)$ is roughly inversely proportional to the stretching $\lambda(t)$. The stretching of a fluid element initially aligned, for example, with the y axis over a switching time τ is $\lambda(\tau) = [(\dot{\gamma}t)^2 + 1]^{1/2}$. Then, over m switching times, the stretching is $\lambda(m\tau) = [(\dot{\gamma}t)^2 + 1]^{m/2}$. This value is roughly equal to the decrease in the striation thickness, $s(0)/s(m\tau)$. If we assume as initial striation thickness $s(0) = 1/2$, i.e. half of the side of the square domain, then the striation thickness at time $t = m\tau$ is

$$s(m\tau) = \frac{1}{2}\left[(\dot{\gamma}\tau)^2 + 1\right]^{-m/2}. \tag{3.3}$$

Figure 2(*b*) shows the estimated striation thickness at the final times $T_f = m\tau = 4, 5, 6, 7, 8$ as a function of the switching time τ. As expected, the striation thickness decreases with increasing final time T_f. However, for a fixed final time T_f, the striation thickness spans several orders of magnitude depending on the value of the switching time τ. For small switching times, i.e. $\tau \leqslant 0.1$, the striation thickness assumes one of its largest values, about 10^{-2}, for all values of T_f. As τ increases, the striation thickness decreases and reaches the minimum at $\tau = 1/\pi \approx 0.315$, which corresponds to the maximum of the stretching efficiency $\langle e_\lambda \rangle_\tau$; see figure 2(*a*). For $\tau \geqslant 1/\pi$, the striation thickness increases with increasing τ; see figure 2(*b*).

It is important to relate the striation thickness to the grid resolution used, $M = 2048$, to guarantee well-resolved numerical simulations. At this resolution, the grid size is $1/2048 \approx 4.8 \times 10^{-4}$. This value is indicated by the horizontal dashed line in figure 2(*b*). As the reference mixer is known to induce striations whose thickness spans several orders of magnitude (Alvarez *et al.* 1998), the thickness of most striations can be

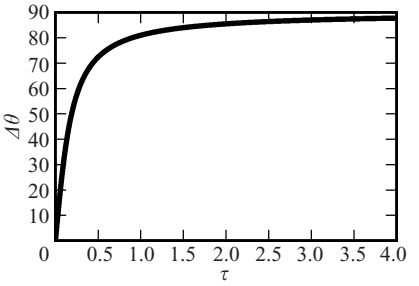

FIGURE 3. The estimate of the change of orientation $\Delta\theta$ induced by the reference mixer over one iteration as a function of the switching time τ.

safely estimated to be at least two orders of magnitude larger than the estimated minimal striation thickness. Therefore, at final times $T_f = 4$ and 5, the grid $M = 2048$ overresolves the scalar field. On the other hand, when the reference mixer operates at switching time $\tau = 1/\pi$, for which the striation thickness is minimal, the final times $T_f = 7$ and 8 appear to be too large for the chosen grid resolution, $M = 2048$. Consequently, we choose $T_f = 6$ as a reasonable final time to be used throughout this study. This value of T_f can be considered a challenge for the mixer because it is expected to produce a homogeneous mixture by advecting particles at most over six characteristic lengths. Note that 30 characteristic lengths are needed to obtain a homogenized mixture with one of the most effective industrially relevant static mixers, the SMX mixer (Paul *et al.* 2004).

We relate the amount of folding to the change of orientation of a fluid element under the stirring action of the velocity field. A simple shear flow with shear rate $\dot{\gamma}$ changes the initial orientation $\theta(0)$ of a fluid element initially aligned, for example, with y axis of an angle

$$\Delta\theta(\tau) = |\theta(\tau) - \theta(0)| = \frac{\pi}{2} - \arctan\frac{1}{\dot{\gamma}\tau}. \tag{3.4}$$

Figure 3 shows that the change of orientation $\Delta\theta(\tau)$ is small at small τ, about 45° when $\tau = 0.15$, about 81° when $\tau = 1.0$ and about 84° when $\tau = 1.5$. The change of orientation asymptotically approaches the value $\theta(\infty) = 90°$. As expected, the longer the shear flow is acting the larger is the change of orientation of a fluid element. However, the reference mixer is particularly efficient in creating folding for $0.5 \leqslant \tau \leqslant 1.0$. For larger switching times, folding is mainly achieved during the first part of the switching time, whereas stretching is mainly induced during the last part. Because stretching induces linear mixing, it follows that the last part of a large switching time is poorly mixing efficient.

We use the above estimates as well as practical considerations to choose a range of operating switching times $[\tau_{min}, \tau_{max}]$ which mimics the operating range of a realistic mixer. For an efficient mixer with an order of magnitude operating range, the switching time, τ_{min}, should be small compared with the characteristic advection time, $T_A = 1$, whereas the switching time, τ_{max}, should be comparable to T_A. Obviously, the switching time value $\tau = 1/\pi$, which corresponds to the maximal stretching efficiency and minimal striation thickness, should lie within the range of operating switching times, i.e. $\tau_{min} \leqslant 1/\pi \leqslant \tau_{max}$. As the smaller operating switching time, we choose $\tau_{min} = 0.1$, which is an order of magnitude smaller than the characteristic advection time. This value is also sufficiently large to prevent a too frequent switching of the velocity

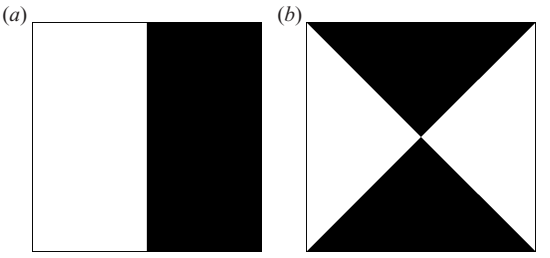

FIGURE 4. (*a*) The 'vertical' and (*b*) the 'envelope' initial configurations of the concentration field. The initial concentration $\varphi(x, y, 0)$ is equal to -1 and $+1$ inside the black and white regions, respectively.

fields, which should be avoided to reduce energy consumption. Moreover, in the case of optimized mixers, which perform optimizations over each switching time, the switching time should be sufficiently large for the computation to be completed successfully. As the larger switching time, we choose $\tau_{max} = 1.3$. This value should be considered a challenge because, as shown above, for switching times larger than unity, the amount of stretching induced by a simple shear flow is much larger than the amount of folding. Moreover, large switching times reduce the number of optimizations performable before reaching the final time and, consequently, reduce the effectiveness of the optimization procedure.

To assess the performance of the reference mixer in terms of its sensitivity to the geometry of the initial configuration of the mixture, we consider two initial configurations, the 'vertical' and the 'envelope', shown in figure 4. The initial concentration $\varphi(x, y, 0)$ is equal to -1 and $+1$ inside the black and white regions, respectively. We named 'vertical' the initial configuration where the white and black fluids are segregated in two equal sized rectangles and the interface is a vertical line. We choose the 'vertical' configuration because it is widely used as an initial condition in literature, and the sine flow performs much better when starting from this initial condition than when starting from a number of differently chosen initial conditions (Gubanov & Cortelezzi 2009). We named 'envelope' the initial configuration where the white and black fluids are segregated in four identical triangles delimited by the two diagonals of the square domain. We choose the 'envelope' configuration because it has been shown (Gubanov & Cortelezzi 2009) that for this initial configuration the reference mixer performs considerably worse than for the 'vertical' and other initial configurations. We quantify the sensitivity of the mixing performance of the reference mixer to the geometry of the initial configuration using the relative sensitivity (Gubanov & Cortelezzi 2009)

$$\delta = \max_{\tau_{min} \leqslant \tau \leqslant \tau_{max}} \left(\frac{|\mu_V(\tau) - \mu_E(\tau)|}{\dfrac{\mu_V(\tau) + \mu_E(\tau)}{2}} \right), \tag{3.5}$$

where $\mu_V(\tau)$ and $\mu_E(\tau)$ are the mix-norm values induced by a mixer at the final time T_f when applied to the 'vertical' and the 'envelope' initial configurations, respectively.

We evaluate the performance of the reference mixer by computing the final values of the mix-norm for the range of switching times $0.1 \leqslant \tau \leqslant 1.3$. This interval is sampled using a switching time step $\Delta\tau = 0.01$ to capture the representative behaviour of the reference mixer. Note that the final mix-norm value is a discontinuous function of τ because the sine flow is known to exhibit sudden bifurcations. However, we

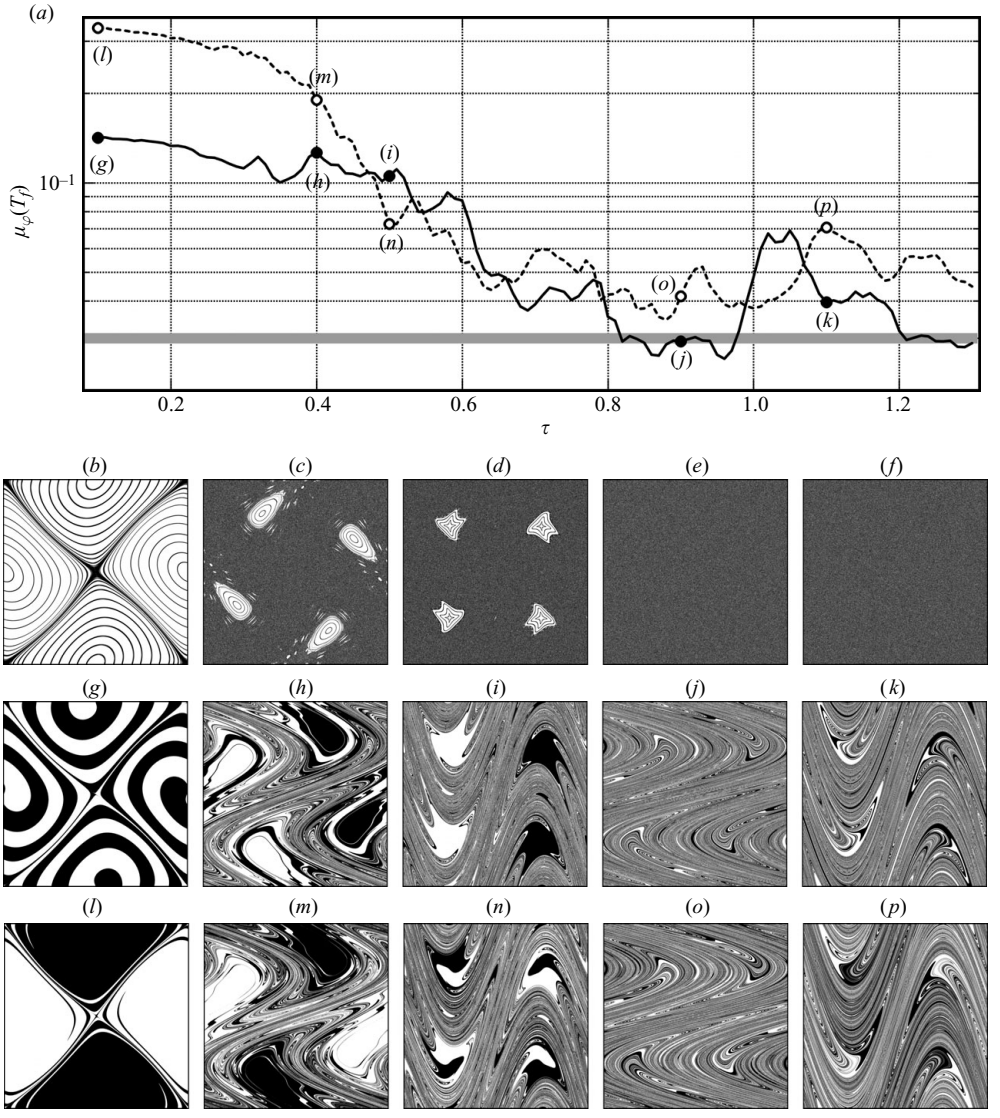

FIGURE 5. (*a*) Value of the mix-norm induced by the reference mixer at time $T_f = 6$ vs. switching time τ for the 'vertical' (solid line) and the 'envelope' (dashed line) initial configurations. The grey horizontal line indicates the target mixing performance. (*b–f*) Poincaré sections of the reference mixer operating at switching time values 0.1 (*b*), 0.4 (*c*), 0.5 (*d*), 0.9 (*e*) and 1.1 (*f*). (*g–k*) Snapshots at time $T_f = 6$ of the concentration field φ stirred by the reference mixer operating at switching time values 0.1 (*g*), 0.4 (*h*), 0.5 (*i*), 0.9 (*j*) and 1.1 (*k*) when applied to the 'vertical' initial configuration. (*l–p*) Snapshots at time $T_f = 6$ of the concentration field φ stirred by the reference mixer operating at switching time values 0.1 (*l*), 0.4 (*m*), 0.5 (*n*), 0.9 (*o*) and 1.1 (*p*) when applied to the 'envelope' initial configuration. The filled circle and the open circle markers within panel (*a*) correspond to the concentration fields (*g–k*) and (*l–p*), respectively.

present the mix-norm value as continuous function of τ for convenience. Figure 5(*a*) shows the values of the mix-norm induced by the reference mixer at time $T_f = 6$ when applied to the 'vertical' (solid line) and the 'envelope' (dashed line) initial configurations, respectively. This figure summarizes and extends several results well known in the literature (Liu *et al.* 1994; Alvarez *et al.* 1998; Muzzio *et al.* 2000; Giona

et al. 2002, 2004; Szalai *et al.* 2003; Phelps & Tucker 2006; Vikhansky & Cox 2007; Cortelezzi *et al.* 2008; Gubanov & Cortelezzi 2009). Clearly, the mixing efficiency of the reference mixer varies considerably over its operating range. The mixer is the least mixing efficient for small switching times, but its efficiency increases as τ increases towards $\tau = 0.8$. The mixer is most efficient when $0.82 \leqslant \tau \leqslant 0.98$ for the 'vertical' initial configuration and when $0.8 \leqslant \tau \leqslant 0.9$ for the 'envelope' configuration. For $\tau \geqslant 1.0$, the mixer becomes less efficient. Figure 5(*a*) also shows that the reference mixer is highly sensitive to the geometry of the initial configuration of the mixture. The value of the relative sensitivity (3.5) is about 85.6 %.

Figure 5(*b–f*) shows Poincaré sections obtained for switching times $\tau = 0.1$ (figure 5*b*), 0.4 (figure 5*c*), 0.5 (figure 5*d*), 0.9 (figure 5*e*) and 1.1 (figure 5*f*). For $\tau = 0.1$, the flow is dominated by two large islands of regular motion which occupy nearly the entire flow domain. For $\tau = 0.4$ and 0.5, there are four islands of regular motion surrounded by a chaotic sea. For $\tau = 0.9$ and 1.1, the chaotic sea invades the entire flow domain, and the islands become undetectable. Because the islands of regular motion form barriers to efficient mixing, the reference mixer is expected to perform poorly for small values of τ, and to perform much better for large values of τ.

Figure 5(*g–p*) shows the instantaneous snapshots of the concentration field induced at time $T_f = 6$ by the reference mixer operating at $\tau = 0.1$, 0.4, 0.5, 0.9 and 1.1 for the 'vertical' and the 'envelope' initial configurations. For $\tau = 0.1$, the reference mixer induces a swirling motion within the two islands of regular motion. The effect of this swirling motion greatly depends on the geometry of the initial conditions. In the case of the 'vertical' initial condition (figure 5*g*), the swirling motion mixes, although poorly, the two fluids because initially they occupy half of each island. In the case of the 'envelope' initial condition (figure 5*l*), the swirling motion is almost unable to mix the two fluids because initially the black fluid is nearly segregated in one island while the white fluid is segregated in the other. For $\tau = 0.4$ and 0.5, the mixer induces four islands of regular motion shown in the Poincaré sections in figure 5(*c*,*d*). The difference in performance between the 'vertical' and the 'envelope' initial configurations can be explained by superimposing the initial configuration onto the corresponding Poincare section and assessing the amount of each fluid contained in each island. For the case $\tau = 0.4$, the reference mixer is more efficient when starting from the 'vertical' initial configuration, while for the case $\tau = 0.5$ it is the opposite; see figure 5(*a*). For $\tau = 0.9$ and 1.1, the Poincaré sections shown in figure 5(*e*,*f*) indicate that asymptotically the reference mixer induces a globally chaotic flow. However, the different values of the mix-norm associated with figure 5(*j*,*k*,*o*,*p*) clearly show that in the case of globally chaotic flows, the asymptotic analysis is of little use to assess the mixing performance of the mixer over short operating times. For the case $\tau = 1.1$, the thicker striations created by stirring the 'envelope' initial configuration contain bigger and better segregated pockets of black and white fluid than in the case of the 'vertical' configuration; see figure 5(*k*,*p*). As a result, for $\tau = 1.1$ the reference mixer performs substantially better for the 'vertical' initial configuration than that for the 'envelope' configuration. A similar, although less pronounced, effect is observed for $\tau = 0.9$; see figure 5(*j*,*o*).

The reference mixer achieves the best performance for the 'vertical' initial configuration when operating within the small range of switching times, $0.82 \leqslant \tau \leqslant 0.98$; see figure 5(*a*). Within this range, the final mix-norm value is about 3×10^{-2}. In this study, we take this performance as the target performance of the mixer. We visualize the target performance with a grey horizontal line in figure 5(*a*) and figures 6(*a*), 10(*a*) and 11(*a*). The goal of this study is to improve and redesign the reference mixer so that the optimal mixer achieves the target performance over

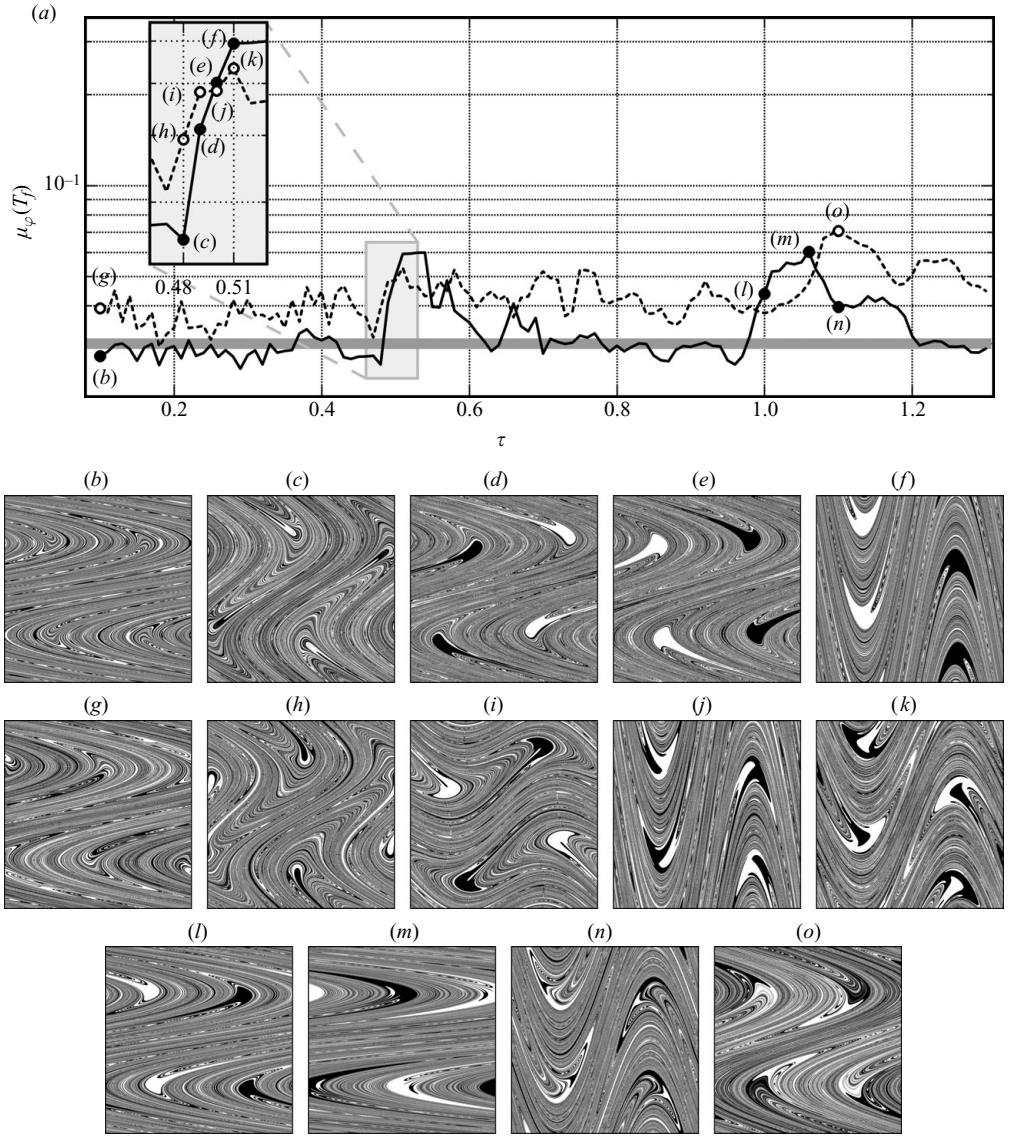

FIGURE 6. Performance of the time-optimized mixer operating at $\eta = 1$ in the purely advective case. (*a*) Value of the mix-norm induced by the mixer at time $T_f = 6$ vs. switching time τ for the 'vertical' (solid line) and the 'envelope' (dashed line) initial configurations. The grey horizontal line indicates the target mixing performance. (*b–o*) Snapshots at time $T_f = 6$ of the concentration field φ stirred by the time-optimized mixer operating at $\eta = 1$ and switching time values 0.1 (*b*, *g*); 0.48 (*c*, *h*); 0.49 (*d*, *i*); 0.5 (*e*, *j*); 0.51 (*f*, *k*); 1.0 (*l*); 1.06 (*m*); and 1.1 (*n*, *o*) when applied to the 'vertical' (*b–f*, *l–n*) and 'envelope' (*g–k*, *o*) initial configurations. The filled circle markers within panel (*a*) correspond to the concentration fields (*b–o*).

the entire range of switching time values $0.1 \leqslant \tau \leqslant 1.3$ for both the 'vertical' and the 'envelope' initial configurations. Note that the target performance is about three times higher than the minimal possible mix-norm value achievable with a checkerboard arrangement of black and white cells. At resolution $M = 2048$, the one used in this study, the minimal possible value of the mix-norm is 1.048×10^{-2}.

4. The time-optimized mixer: the effect of protocol optimization

The most intuitive and obvious approach to increasing the performance of the reference mixer is the optimization of the stirring protocols. In this approach, the periodic protocols are replaced by more mixing efficient aperiodic protocols generated by an optimization procedure. As noted by Liu *et al.* (1994), aperiodic protocols do not present periodic points and, consequently, flows stirred by such protocols are free of islands of regular motion. However, it is not trivial to find a mixing efficient aperiodic protocol. Cortelezzi *et al.* (2008) have shown, using the mix-norm as a diagnostic, that there is a large percentage of aperiodic protocols that do not stir efficiently.

Because the early stages of mixing are dominated by advection, it is essential for a protocol to be efficient especially during the initial stirring phase. We solve the protocol optimization problem using the branch-and-bound approach (Lawler & Wood 1966). A reasonable bounding criterion is that a protocol is likely to be mixing efficient if it begins with a mixing efficient sub-protocol. Note that although this criterion is based on a heuristic argument, it leads to a computationally efficient optimization procedure able to generate protocols with nearly optimal performance (Cortelezzi *et al.* 2008).

Given the above criterion, we implement the branch-and-bound approach for a switching time τ and a final time $T_f = N\tau$ as follows: First, we consider all possible sub-protocols that consist of η iterations, where the integer parameter η, a sub-multiple of N, is the switching time horizon. For each of these sub-protocols, we compute the solution to the purely advective problem (2.3) starting at $t = 0$ and using, for all protocols, the same initial condition $\varphi(x, y, 0)$ up to one time horizon, $t = \eta\tau$. Then, we evaluate the mixing efficiency of these sub-protocols by computing the mix-norm of each solution, $\varphi(x, y, \eta\tau)$. The sub-protocol which induces the lowest mix-norm is optimal and is selected. Finally, we reduce the set of possible protocols to the set of protocols starting with the best-performing sub-protocol. As a result, we reduce the number of possible solutions from 2^N to $2^{N-\eta}$ at the computational cost of evaluating only 2^η sub-protocols of η iterations. To further reduce the number of possible solutions, we recursively apply the branch-and-bound approach to the reduced set of possible protocols. That is, the concentration field $\varphi(x, y, \eta\tau)$ induced by the selected optimal sub-protocol is used as the initial condition for the optimization over the next time horizon, $\eta\tau \leqslant t < 2\eta\tau$, and so on until the final time T_f is reached. The total number of short time horizon optimizations needed to reach the final time T_f is $m = T_f/\eta\tau$. The m optimal sub-protocols concatenated together form a suboptimal stirring protocol, which is referred to as a short time horizon optimal protocol (Cortelezzi *et al.* 2008).

We improve the design of the reference mixer by implementing the above described optimization procedure. The resulting *time-optimized mixer* in general computes a different short time horizon optimal protocol for any given choice of the initial configuration of the mixture and the switching time τ. The performance of the time-optimized and reference mixers can be meaningfully compared because both mixers use the same actuating system and, consequently, induce stirring velocity fields with the same shear rate and power input (2.2).

In order to characterize the performance of the time-optimized mixer, we first estimate the computational cost required to operate it. For each one of the m optimizations needed to reach the final time T_f, the short time horizon optimization procedure evaluates 2^η sub-protocols. The map (2.4) is applied for η iterations at the

first optimization, for 2η iterations at the second optimization, and so on until the final optimization for which $m\eta$ iterations are needed. Consequently, the computational cost of evaluating 2^η sub-protocols for all m optimizations is

$$C = \sum_{k=1}^{m} 2^\eta k\eta = N(N+\eta)2^{\eta-2}. \tag{4.1}$$

It follows that the computational cost grows exponentially with η and quadratically with N. In the limiting case of $\eta = N$, the short time horizon optimization procedure performs an exhaustive search among all admissible protocols, and the computational cost is $C = 2^{N-1}N^2$. Note that the computational cost of an exhaustive search grows exponentially with N, whereas the cost of the short time horizon optimization procedure grows exponentially with η. Therefore, for small values of η, the short time horizon optimization procedure is exponentially more cost-efficient than the exhaustive search for the best-performing protocol.

We now evaluate the performance of the time-optimized mixer when the smallest possible value of the switching time horizon, $\eta = 1$, is selected. We made this choice because it has been shown that protocols optimized over very short time horizons are competitively mixing efficient with respect to protocols optimized over longer time horizons (Cortelezzi *et al.* 2008). In this case, because the time horizon is equal to one switching time τ, the optimization procedure simply chooses the best-performing of the two velocity fields $\boldsymbol{v}_0$ and $\boldsymbol{v}_1$. Therefore, setting $\eta = 1$ results in the most cost-effective short-time-horizon optimization of a stirring protocol, whose cost is $C = N(N+1)/2$.

Figure 6(a) shows the values of the mix-norm induced by the time-optimized mixer at time $T_f = 6$ when applied to the 'vertical' (solid line) and the 'envelope' (dashed line) initial configurations. As it can be seen by comparing figures 5(a) and 6(a), the mixing efficiency of the time-optimized mixer is substantially better than the efficiency of the reference mixer for small/medium values of the switching time τ. However, for large values of the switching time, $\tau \geqslant 0.8$, the time-optimized mixer generates nearly periodic stirring protocols and, consequently, the time-optimized mixer and reference mixers induce similar final values of the mix-norm. This is not surprising because for large switching times, stirring over two or more consecutive iterations with the same velocity field results in a lack of folding and an unnecessary amount of stretching, which contributes to mixing linearly in time. Therefore, the cost of operating the time-optimized mixer at large switching times is unjustified. Unexpectedly, a closer analysis of the performance of the time-optimized mixer shows that it deteriorates substantially in the intervals $0.5 \leqslant \tau \leqslant 0.6$ and $1.0 \leqslant \tau \leqslant 1.2$. Figure 6($a$) also shows that the time-optimized mixer is clearly less sensitive to the geometry of the initial configuration than the reference mixer. The relative sensitivity (3.5) of the time-optimized mixer is about 64.6 %, which is less than $\delta = 85.6\,\%$ computed for the reference mixer. Overall, the mixing efficiency of the time-optimized mixer is closer to the target performance but still insufficiently uniform and insensitive to the geometry of the initial configuration.

It is insightful to relate the mixing efficiency of the time-optimized mixer to the geometrical structure of the concentration field. Figure 6(b–k) shows the instantaneous snapshots of the concentration field induced at time $T_f = 6$ by the time-optimized mixer operating at $\tau = 0.1$, 0.48, 0.49, 0.5 and 0.51 when applied to the 'vertical' and the 'envelope' initial configurations, respectively. For switching times $\tau = 0.1$ and 0.48, the mixer induces fine striations over the entire mixing domain for both initial

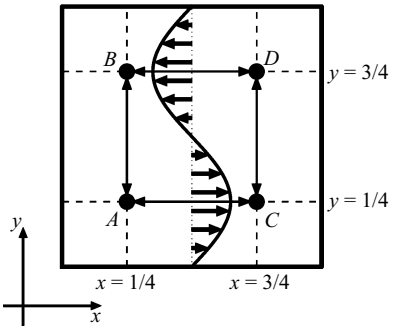

FIGURE 7. Lines of zero shear induced by the velocity fields (2.1) and the four points, A, B, C and D, around which pockets of unmixed fluid form when the reference and time-optimized mixers operate at $\tau = 0.5$.

configurations. The best mixing efficiency is achieved in the case of the 'vertical' initial configuration, as indicated by markers labelled (b) and (c) placed on the solid line in figure 6(a). For switching times $\tau = 0.49$, 0.50 and 0.51, surprisingly, all the concentration fields contain four pockets of black and white fluids surrounded by a well-mixed region. As τ increases from 0.49 to 0.51, the size of the pockets increases; see figures 6(d–f) and 6(i–k). This results in a sharp and unexpected increase of the final mix-norm values at $\tau \approx 0.5$, as shown in figure 6(a). The jump in performance of the time-optimized mixer is particularly evident in the case of the 'vertical' configuration.

Figure 6(a) also shows that the performance of the time-optimized mixer worsens noticeably when it operates within the range $1.0 \leqslant \tau \leqslant 1.2$. In the case of the 'vertical' initial configuration, there is a sudden increase in the mix-norm value in the interval $0.98 \leqslant \tau \leqslant 1.10$; see the solid line in figure 6(a). In fact, when operating at $\tau = 1.0$, the time-optimized mixer induces four pockets of black and white fluids; see figure 6(l). In the case of the 'envelope' initial configuration, the sudden increase in the mix-norm value occurs within the range $1.06 \leqslant \tau \leqslant 1.17$. The mixer is the worst-performing when operating at $\tau = 1.1$, see the dashed line in figure 6(a), when the corresponding concentration field presents four large pockets containing both black and white fluids; see figure 6(o).

Unlike the case of the reference mixer, the pockets of segregated fluid present at operating conditions $0.5 \leqslant \tau \leqslant 0.6$ and $1.0 \leqslant \tau \leqslant 1.2$ cannot be induced by the presence of islands of regular motion because the optimized protocols are aperiodic for these values of τ. Then what causes the pockets of unmixed fluid shown in figures 6(d–f), 6(i–k) and 6(l–o)? To answer this question, we note that for any value of the switching time, the stirring velocity field $\boldsymbol{v}_0$ (2.1) induces zero shear along the lines $y = 1/4$ and $y = 3/4$; see figure 7. Thus, fluid elements located near these lines are merely advected by $\boldsymbol{v}_0$ while undergoing almost negligible deformations. Similarly, the stirring velocity field $\boldsymbol{v}_1$ (2.1) induces zero shear along the lines $x = 1/4$ and $x = 3/4$ and results in only minor deformations of the fluid elements located in the vicinity of these lines. Let consider the set $S = \{A, B, C, D\}$ of the cross points of the four lines described above; see figure 7. Clearly, for $\tau = 0.5$ this set is invariant with respect to any admissible stirring protocol. Thus, the fluid particles which initially belong to S remain in S, i.e. on the lines of zero shear for all times. Moreover, the fluid elements initially located near S remain in the vicinity of S because of the nearly zero shear induced by the velocity fields $\boldsymbol{v}_0$ and $\boldsymbol{v}_1$. In other words, the neighbourhood of S remains almost invariant

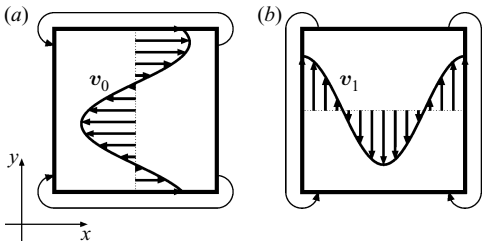

FIGURE 8. The schematic of the mixing device equipped with the new actuating system defined by velocity fields (5.1). (*a*,*b*) The stirring velocity fields $\boldsymbol{v}_0$ shifted by $\psi = 0.333$ and $\boldsymbol{v}_1$ shifted by $\psi = 0.25$. The curves joining the opposite sides of the square mixing domain indicate periodic boundary conditions.

over the finite time interval $[0, T_f]$ with respect to any admissible stirring protocol. For a detailed discussion of almost-invariant sets, the reader is referred to the work of Froyland & Padberg (2009). Our computations also show that pockets of unmixed fluids emerge even when operating the time-optimized mixer at the more expensive switching time horizons $\eta = 4$ and 8. At switching times close but not equal to 0.5, the set S and its neighbourhood are almost invariant, which results in the pockets of unmixed fluids. Therefore, these pockets emerge because of the mechanical limitations of the actuating device which generates almost-invariant sets around the points A, B, C and D. The poor performance of the time-optimized mixer when operating at switching times $1.0 \leqslant \tau \leqslant 1.2$ can be explained by a similar argument because the switching time $\tau = 0.5$ is a sub-multiple of $\tau = 1.0$. Consequently, it is necessary to redesign the actuating device to prevent the formation of almost-invariant sets and improve the performance of the mixer over the ranges $0.5 \leqslant \tau \leqslant 0.6$ and $1.0 \leqslant \tau \leqslant 1.2$. Note that points similar to those shown in figure 7 have been reported by Finn, Thiffeault & Gouillart (2006). However, these points do not generate pockets of unmixed fluids because they lie in the regions of the mixing domain where the shear rate is not zero.

5. Space-optimized mixer: the effect of velocity profile optimization

In § 4, we have shown the mechanical limitations of the actuating system used to stir the mixture by the reference and time-optimized mixers. In this section, we introduce a new actuating system capable of generating stirring velocity fields able to induce non-zero shear stresses in every chosen point of the mixing domain. We will show that the new actuating system addresses the weaknesses of the old one.

We find inspiration for modifying the actuating system in a number of previous studies (Pierrehumbert 1994, 2000; Antonsen *et al.* 1996; Thiffeault *et al.* 2004; Shaw *et al.* 2007; O'Naraigh & Thiffeault 2008) in which the stirring velocity fields of the sine flow were shifted along the associate coordinate axis; see figure 8. In these studies, the phase shift of the velocity profile is randomly chosen at each iteration so as to eliminate the flow periodicity. It was shown that a random phase shift of the velocity profiles effectively suppresses the islands of regular motion that emerge in the periodic sine flow.

Thus motivated, we redesign the actuating system of the reference mixer so that the new actuator is able to produce a stirring velocity field shifted by an intelligently chosen phase. Mathematically, the redesign is equivalent to adding a phase shift ψ to

the original velocity fields (2.1), i.e.

$$\boldsymbol{v}_0(x, y) = [\sin(2\pi(y + \psi)), 0]^*, \quad \boldsymbol{v}_1(x, y) = [0, \sin(2\pi(x + \psi))]^*. \tag{5.1}$$

The mixing device equipped with the new actuating system is visualized in figure 8. Because the velocity profiles (5.1) are periodic in ψ with period 1, without loss of generality we restrict the phase shift ψ to the interval $[0, 1)$. The stirring velocity fields (2.1) generated by the old actuating system can be recovered by setting ψ to zero in (5.1). As ψ is varied in the range $[0, 1)$, the profiles of the velocity fields $\boldsymbol{v}_0$ and $\boldsymbol{v}_1$ are rigidly translated along y and x axes, respectively (see figure 8) and are able to induce a non-zero shear rate at any given point within the mixing domain. Note that the old and new actuators use the same amount of power input (see (2.2)) and deliver the same shear rate. The difference is that the new actuator can deliver the requested amount of shear at intelligently chosen points, while the old actuator is forced to deliver a predefined level of shear always at the same point.

The addition of the phase shift to the stirring velocity fields requires the modification of the solution procedure for the purely advective sine flow problem. The map (2.4) is replaced by the map

$$\begin{pmatrix} X_{m-1}^{i,j} \\ Y_{m-1}^{i,j} \end{pmatrix} = \begin{cases} \begin{pmatrix} X_m^{i,j} - \tau \sin[2\pi(Y_m^{i,j} + \psi_m)] \\ Y_m^{i,j} \end{pmatrix} \bmod 1, & \text{if} \quad \alpha_m = 0, \\ \begin{pmatrix} X_m^{i,j} \\ Y_m^{i,j} - \tau \sin[2\pi(X_m^{i,j} + \psi_m)] \end{pmatrix} \bmod 1, & \text{if} \quad \alpha_m = 1, \end{cases} \tag{5.2}$$

where $\{\psi_m\}_{m=1}^N$ are the phase shifts used at iterations $1, \ldots, N$.

In order to test the new mixer and compare it with the reference mixer, the mixture is stirred using a periodic protocol. The phase shift ψ of the stirring velocity field (5.1) is optimized by selecting at each iteration the phase shift that induces the lowest possible value of the mix-norm. We refer to this type of optimization as the *phase optimization* and call the resulting mixing device the *space-optimized mixer*. The latter name reflects the nature of the phase optimization, whereby different values of ψ alter the spatial distribution of the shear rate exerted by velocity fields (5.1) within the mixing domain.

The problem of finding the optimal value of the phase shift is a continuous optimization problem because ψ can assume any real value within the range $[0, 1)$. We use as a cost function the mix-norm, as in the case of the time-optimized mixer. Numerical experiments indicate that the cost function is continuous in ψ; see figure 9 for an example. Therefore, the problem of finding the optimal phase shift can be solved by using one of the conventional continuous optimization methods. We choose the derivative-free pattern search method (see Lewis & Torczon 2000, and references therein), which is implemented in the APPSPACK library (see Kolda 2005 and references therein), because of the lack of analytic expressions for the derivatives of the cost function.

For a given switching time τ and a final time $T_f = N\tau$, the phase optimization generates a periodic sequence of the optimal velocity profiles $\boldsymbol{v}_0(\psi_1)$, $\boldsymbol{v}_1(\psi_2)$, $\boldsymbol{v}_0(\psi_3)$, ... At each iteration, the optimal velocity profile $\boldsymbol{v}_0(\psi_k)$ or $\boldsymbol{v}_1(\psi_k)$ corresponds to a sinusoidal profile shifted by a value of the phase ψ_k, which minimizes the mix-norm of the concentration field over the kth switching time. Starting at $t = 0$ with a given initial configuration of the mixture, the pattern search method (Lewis & Torczon

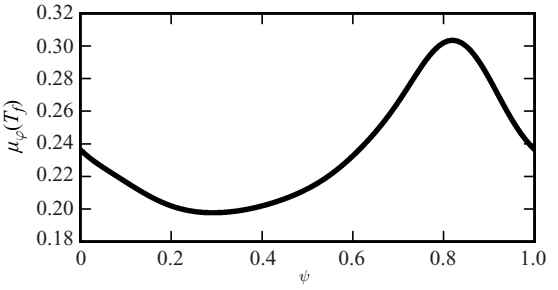

FIGURE 9. Typical structure of the cost function minimized by the phase optimization procedure.

2000) is used to find the optimal value of the phase shift ψ_1 for the velocity field $\boldsymbol{v}_0$. The concentration field $\varphi(x, y, \tau)$ induced by the velocity field $\boldsymbol{v}_0(\psi_1)$ is then used as the initial condition for the optimization over the next switching time, $\tau \leqslant t < 2\tau$, and so on until the final time, $T_f = N\tau$, is reached. As a result, the space-optimized sequence of the stirring velocity fields is prescribed by the periodic protocol and the sequence of the optimal phase shifts, $\psi_1, \psi_2, \ldots, \psi_N$.

To characterize fully the performance of the space-optimized mixer, we estimate the computational cost required to operate it. Consistently with the cost estimation presented in § 4, we perform our estimation in terms of the total number of iterations, N, the switching time, τ, and the average number P of evaluations of the cost function per iteration. In the purely advective case, the map (5.2) is applied on average P times for one iteration at the first iteration, for P times for two iterations at the second iteration, and so on until the final iteration. Consequently, the computational cost of the optimization is

$$C = \sum_{k=1}^{N} kP = P\frac{N(N+1)}{2}. \tag{5.3}$$

It follows that the computational cost grows linearly with P and quadratically with N. Numerical computations performed in this work show that an average of $P = 13$ evaluations of the cost function is sufficient to determine the optimal phase shift with a relative accuracy of 1 %. The resulting computational cost of the space-optimized mixer is 13 times more expensive than that of the time-optimized mixer operating at $\eta = 1$ and becomes comparable with the computational cost of the time-optimized mixer operating at $\eta = 5$.

To characterize the mixing performance of the space-optimized mixer, we compare it with the performance of the reference and time-optimized mixers. We begin with the comparison with the reference mixer. Figure 10(a), which shows the values of the mix-norm induced by the space-optimized mixer at time $T_f = 6$ when applied to the 'vertical' (solid line) and the 'envelope' (dashed line) initial configurations, should be compared with figure 5(a). The improvement in performance is striking and shows the impact of the new actuating system and optimization procedure on the performance of the space-optimized mixer. The space-optimized mixer nearly delivers the target performance over the range of operating conditions $\tau \in [0.5, 1.3]$. At low values of τ, i.e. $\tau \in [0.1, 0.4]$, the performance of the space-optimized mixer deteriorates visibly. Furthermore, the spread of the solid and the dashed lines in figures 10(a) and 5(a) shows that the space-optimized mixer is much less sensitive than the reference mixer to the geometry of the initial concentration field. The value

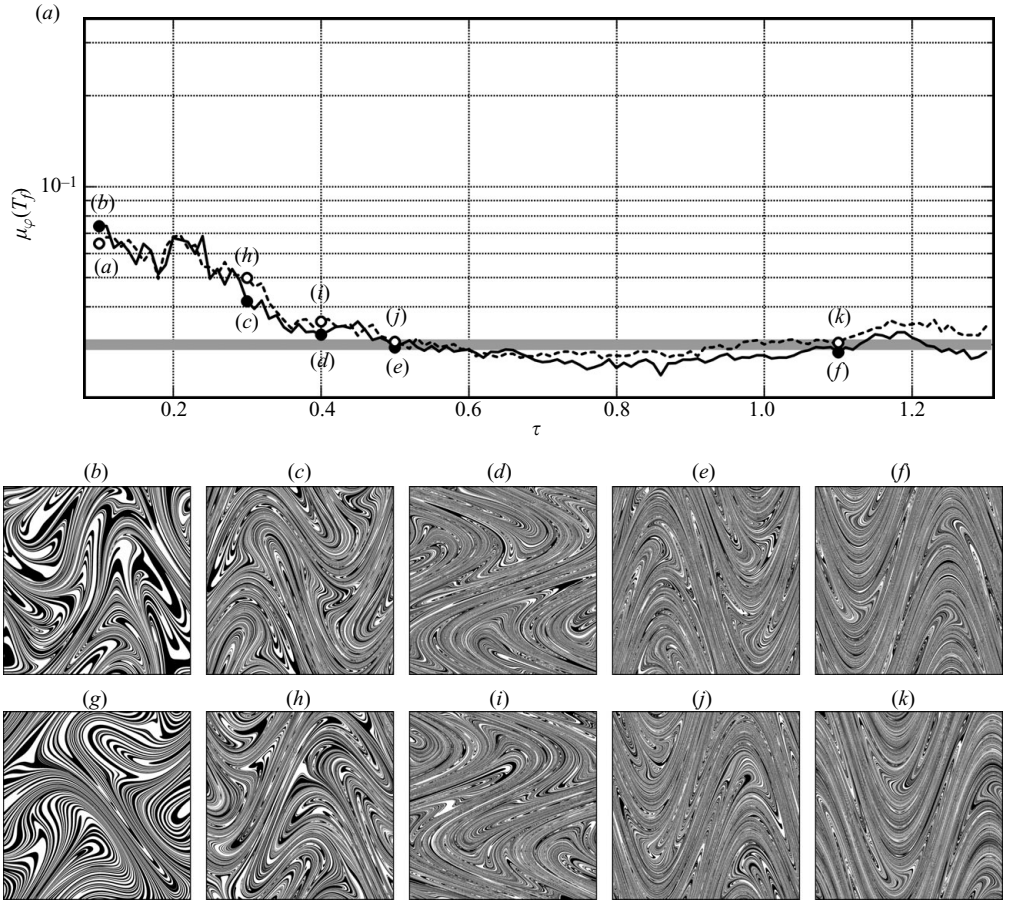

FIGURE 10. Performance of the space-optimized mixer in the purely advective case. (*a*) Value of the mix-norm induced by the mixer at time $T_f = 6$ vs. switching time τ for the 'vertical' (solid line) and the 'envelope' (dashed line) initial configurations. The grey horizontal line indicates the target mixing performance. (*b–k*) Snapshots at time $T_f = 6$ of the concentration field φ stirred by the space-optimized mixer operating at switching time values 0.1 (*b*),(*g*); 0.3 (*c*, *h*); 0.4 (*d*, *i*); 0.5 (*e*, *j*) and 1.1 (*f*, *k*) when applied to the 'vertical' (*b–f*) and 'envelope' (*g–k*) initial configurations. The filled circle markers and the open circle markers within panel (*a*) correspond to the concentration fields (*b–f*) and (*g–k*), respectively.

of the relative sensitivity (3.5) is about 23.2 % for the space-optimized mixer, which is considerably less than $\delta = 85.6$ % for the reference mixer.

We now compare the mixing performance of the space- and time-optimized mixers, figure 10(*a*) and figure 6(*a*), respectively. The performance of the space-optimized mixer is clearly more consistent than the erratic performance of the time-optimized mixer. In particular, the space-optimized mixer, thanks to the new actuating system, nearly delivers the target performance within the range $\tau \in [0.5, 1.3]$, while the performance of the time-optimized mixer visibly deteriorates in the ranges $\tau \in [0.5, 0.6]$ and $\tau \in [1.0, 1.2]$ as a result of the mechanical limitation of the old actuating system. However, the mixing performance of the time-optimized mixer is visibly better than the performance of the space-optimized mixer in the low range of operating conditions, i.e. $\tau \in [0.1, 0.4]$. The space-optimized mixer is also considerably less sensitive to the geometry of the initial concentration field than

the time-optimized mixer. The relative sensitivity for the space-optimized mixer, $\delta = 23.2\,\%$, is considerably less than $\delta = 64.6\,\%$ for the time-optimized mixer.

Figures 10(*b–k*) and 6(*b–k*) show the final concentration fields induced by the space- and time-optimized mixers at the final time $T_f = 6$ when applied to the 'vertical' and the 'envelope' initial configurations, respectively. In the low range of operating conditions, $\tau \in [0.1, 0.4]$, where the reference mixer induces islands of regular motion, the space-optimized mixer struggles to avoid the formation of such structures. It seems that the space-optimized mixer, which is constrained to use a periodic protocol, avoids the formation of the islands of regular motion mostly by favouring folding over stretching, as it is shown by the convoluted geometry with thick lamellae of the concentration field; see figures 10(*b*) and 10(*g*) for the case $\tau = 0.1$. In the medium–high range of operating conditions, i.e. for $\tau \geqslant 0.5$, the geometry of the concentration field induced by the space-optimized mixer shows thin striations with little segregation of white or black fluids; see figure 10(*e*,*f*,*j*,*k*). These figures show a remarkable improvement with respect to the time-optimized mixer in the ranges $0.5 \leqslant \tau \leqslant 0.6$ and $1.0 \leqslant \tau \leqslant 1.2$.

The performance deterioration of the space-optimized mixer for low switching times can be related to the performance deterioration of the reference mixer. In fact, these mixers share the same periodic stirring protocol, which is known to be mixing-inefficient for small values of the switching time. Therefore, we can expect to improve the mixing efficiency of the space-optimized mixer by optimizing its stirring protocols.

6. Optimal mixer: coupled time and space optimizations

The time- and space-optimized mixers presented in the previous sections leverage two totally different optimization philosophies. The former optimizes the protocol by forecasting the future, while the latter optimizes the local delivery of the shear rate. They both have strengths and weaknesses. Because the two optimization procedures are completely uncoupled, it is natural to explore the advantages of coupling them in an attempt to produce a better optimization procedure.

We design the optimal mixer by implementing on the mechanical configuration of the space-optimized mixer a coupled optimization procedure as follows. At each iteration, we perform a two-step procedure. First, we find the optimal phase shifts for both stirring velocity fields $\boldsymbol{v}_0$ and $\boldsymbol{v}_1$. Second, we select the best-performing of the two optimal velocity fields. Clearly, the computational cost of the coupled optimization is twice as large as the cost of the space optimization; see estimate (5.3).

Figure 11(*a*) summarizes the performance of the optimal mixer in the purely advective case. The mixer is able to deliver the target performance over nearly the entire operating range $0.1 \leqslant \tau \leqslant 1.3$. Only for large values of τ the performance is slightly above the target performance. Moreover, the optimal mixer is nearly insensitive to the initial geometry of the concentration field. Its relative sensitivity is $\delta = 20.4\,\%$, which is considerably less than $\delta = 64.6\,\%$ for the time-optimized mixer and even less than $\delta = 23.2\,\%$ for the space-optimized mixer.

Figure 11(*b–k*) shows the snapshots at the final time $T_f = 6$ of the concentration field φ stirred by the optimal mixer when applied to the 'vertical' (figure 11*b–f*) and 'envelope' (figure 11*g–k*) initial configurations. For $\tau = 0.1$, which corresponds to almost the worst performance of the space-optimized mixer, the optimal mixer is able to induce less convoluted and thinner striations than the space-optimized mixer thanks to the protocol optimization; see figures 11(*b*,*g*) and 10(*b*,*g*). For $\tau = 0.5$, which

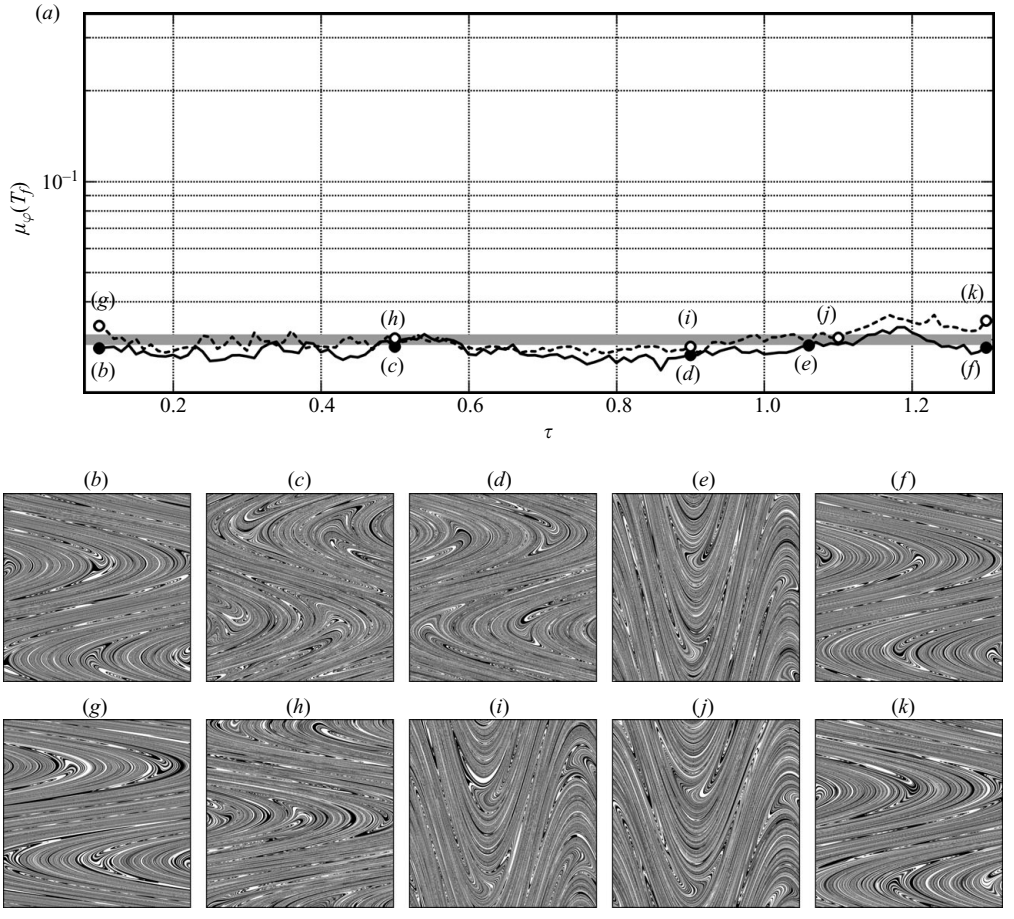

FIGURE 11. Performance of the optimal mixer. (*a*) The value of the mix-norm induced by the mixer at time $T_f = 6$ when applied to the 'vertical' (solid line) and the 'envelope' (dashed line) initial configurations. The grey horizontal line indicates the target performance. (*b–k*) Snapshots at time $T_f = 6$ of the concentration field φ stirred by the optimal mixer at switching time values 0.1 (*b*, *g*); 0.5 (*c*, *h*); 0.9 (*d*, *i*); 1.06 (*e*); 1.1 (*j*); 1.3 (*f*, *k*) when applied to the 'vertical' (*b–f*) and 'envelope' (*g–k*) initial configurations. The filled circle markers and the open circle markers within panel (*a*) correspond to the concentration fields (*b–f*) and (*g–k*), respectively.

corresponds to almost the worst performance of the time-optimized mixer caused by the presence of pockets of segregated fluids (see figure 6*e* and 6*j*), the optimal mixer induces final concentration fields free of pockets thanks to the phase optimization (see figures 11*c* and 11*h*). For $\tau = 0.9$, which corresponds to the best mixing performance of the reference mixer, the optimal mixer slightly improves the performance and induces final concentration fields similar to the concentration fields induced by the reference mixer; see figures 11(*d*,*i*) and 5(*j*,*o*). For $\tau = 1.06$ and 1.1, which correspond to the worst performance of the time-optimized mixer when applied to the 'vertical' and 'envelope' initial configurations, respectively (see figure 6*a*), thanks to the phase optimization, the final mix-norm induced by the optimal mixer is nearly a flat line, see figure 11(*a*).

The optimal mixer is the least mixing efficient when it operates at $\tau = 1.3$ and is applied to the 'envelope' initial configuration; see the open circle marker (k) in figure 11(a). For this value of the switching time, the optimal mixer is also most sensitive to the geometry of the initial concentration field; see figures 11(f) and 11(k). The deterioration of the mixing performance within the range $1.0 \leqslant \tau \leqslant 1.3$ is observed for any of the mixing devices considered in this study; see figures 5(a), 6(a), 10(a) and 11(a). Although in the case of the optimal mixer this deterioration in performance is less pronounced than that for the other mixers, it persists. This can be explained recalling that for large switching times, $1.0 \leqslant \tau \leqslant 1.3$, all mixers produce an insufficient amount of folding and an excessive amount of stretching. The deterioration in performance for $1.0 \leqslant \tau \leqslant 1.3$ also agrees with the estimated stretching efficiency, striation thickness and folding obtained in § 3. As τ increases from 1.0 to 1.3, the estimated stretching efficiency decreases (see figure 2a), the estimated striation thickness increases (see figure 2b) and the amount of folding remains nearly the same (see figure 3). Nevertheless, the optimal mixer is still able to significantly improve the mixing performance when compared with the reference mixer even for large switching times, thanks to the phase optimization.

7. Summary and conclusions

In this study, we considered the conceptual problem of designing an optimal mixer, a mixing device able to deliver a uniform and optimal mixing performance within its entire operating range and for a wide range of initial configurations of the mixture. We described the sequence of steps needed to derive an optimal mixer starting from a reference mixing device.

As a reference mixer, we considered the sine flow. We characterized the stretching efficiency and the rate of folding of the reference mixer and determined its operating range. As a measure of mixing efficiency, we used the mix-norm. We showed that the reference mixer is highly mixing efficient only within a small sub-range of operating conditions. Within the low range of operating conditions, the reference mixer performs poorly because of the islands of regular motion that emerge under the action of its periodic stirring protocol. Within the high range of operating conditions it performs poorly, because it induces an insufficient amount of folding and an excessive amount of stretching. Moreover, we showed that the mixing performance of this mixer strongly depends on the initial configuration of the mixture. We selected the best mixing efficiency delivered by the reference mixer as the target performance to be achieved by the optimal mixer over the entire operating range.

Our first step towards the design of an optimal mixer was to replace the periodic stirring protocols used by the reference mixer with optimized aperiodic protocols obtained using the short time horizon optimization procedure. As a cost function for this optimization, we used the mix-norm. We observed that the resulting mixing device, the time-optimized mixer, performed substantially better than the reference mixer but within two windows of operating conditions. We showed that the deterioration in performance of the time-optimized mixer within these two windows is caused by the mechanical limitations of the actuating system. We also noted that over the high range of operating conditions, the short time horizon procedure generates stirring protocols that are nearly periodic, and thus optimization of a stirring protocol within this range becomes ineffective. Finally, we observed that the time-optimized mixer is still too sensitive to the geometry of the initial configuration of the mixture, although considerably less sensitive than the reference mixer.

Our second step towards the design of the optimal mixer was to redesign the actuating system of the reference mixer so as to address its mechanical limitations. We introduced a new actuating system able to generate stirring velocity fields that are shiftable along their reference axis and an optimization procedure able to select at each iteration the phase shift that is the most mixing efficient. We used the mix-norm as the cost function for the optimization. We tested the space-optimized mixer with a periodic protocol. This mixer nearly delivers the target performance over a range from medium to high operating conditions. However, within the low range of operating conditions, we observed a deterioration in performance caused by the periodic stirring protocol, which generates an insufficient amount of stretching and an excessive amount of folding. Finally, we showed that the space-optimized mixer is nearly insensitive to the geometry of the initial configuration.

Our final step towards the design of the optimal mixer was to couple the time and the phase optimizations within a mixing device equipped with the new actuating system. We obtained an optimal mixer. We observed that the optimal mixer is highly mixing efficient within the entire range of operating conditions which spans over more than one order of magnitude. It achieves the target performance in only six characteristic advection times. Moreover, the optimal mixer is nearly insensitive to different geometries of the initial configuration of the mixture.

The optimal mixer is able to overcome two of the major problems affecting the mixing performance of many industrially relevant mixers. Namely, the non-uniformity of the mixing performance owes to (i) different operating conditions and (ii) different configurations of the mixture injected into the mixing device. We showed that these two problems can be conceptually addressed by combining two simple optimizations: the optimization of the stirring protocol over very short horizons and the optimization of the profiles of the stirring velocity fields. These two optimizations complement each other. The optimization of the stirring protocol effectively controls in time the amounts of stretching and folding induced by the mixing device. In particular, in the low range of operating conditions of the sine flow, this optimization avoids excessive folding and promotes stretching. The optimization of the profiles of the stirring velocity fields controls the spatial distribution of stretching within the mixing domain by delivering the highest shear rate to the regions that need it most. In particular, this optimization remarkably enhances the mixing performance within medium and high ranges of operating conditions of the sine flow. Moreover, this optimization nearly eliminates the sensitivity of the mixer to the initial geometrical configuration of the mixture.

Certainly, with the current state of technology, the above two optimizations cannot be directly applied to the complex flows observed in applications. How to predict realistic complex flows and flows of non-Newtonian fluids? How to evaluate the homogenization quality of an inherently three-dimensional concentration field? How to change efficiently the shapes of the profiles of the stirring velocity fields, and what shapes to choose? Our work provides an estimate of the potential improvements to the mixing performance achievable combining the optimization of the stirring protocol and the profiles of the stirring velocity fields. Our results indicate that without implementing these procedures, one should expect a dramatic decrease in the mixing performance for certain ranges of operating conditions and for some configurations of the mixture injected into the mixing device.

Funding was provided by NSERC under a Postgraduate Scholarship and under contract RGPIN217169.

REFERENCES

Adrover, A., Cerbelli, S. & Giona, M. 2002 A spectral approach to reaction/diffusion kinetics in chaotic flows. *Comput. Chem. Engng* **26**, 125–139.

Alvarez, M. M., Muzzio, F. J., Cerbelli, S., Adrover, A. & Giona, M. 1998 Self-similar spatiotemporal structure of intermaterial boundaries in chaotic flows. *Phys. Rev. Lett.* **81**, 3395–3398.

Antonsen, Jr., T. M., Fan, Z., Ott, E. & Garcia-Lopez, E. 1996 The role of chaotic orbits in the determination of power spectra of passive scalars. *Phys. Fluids* **8**, 3094–3104.

Aref, H. 1984 Stirring by chaotic advection. *J. Fluid Mech.* **143**, 1–21.

Aref, H. 2002 The development of chaotic advection. *Phys. Fluids* **14**, 1315–1325.

Aref, H. & El Naschie, M. S. (Eds.) 1995 *Chaos Applied to Fluid Mixing*. Pergamon.

Cerbelli, S., Alvarez, M. M. & Muzzio, F. J. 2002 Prediction and quantification of micromixing intensities in laminar flows. *Am. Inst. Chem. Eng. J.* **48**, 686–700.

Cortelezzi, L., Adrover, A. & Giona, M. 2008 Feasibility, efficiency and transportability of short horizon optimal mixing protocols. *J. Fluid Mech.* **597**, 199–231.

Cunha, A. G., Covas, J. A. & Oliveira, P. 1998 Optimization of polymer extrusion with genetic algorithms. *IMA J. Math. Appl. Bus. Indus.* **9**, 267–277.

D'Alessandro, D., Dahleh, M. & Mezić, I. 1999 Control of mixing in fluid flow: a maximum entropy approach. *IEEE Trans. Autom. Control* **44**, 1852–1863.

Finn, M. D., Cox, S. M. & Byrne, H. M. 2004 Mixing measures for a two-dimensional chaotic stokes flow. *J. Engng Math.* **48**, 129–155.

Finn, M. D., Thiffeault, J.-L. & Gouillart, E. 2006 Topological chaos in spatially periodic mixers. *Physica* D **221**, 92–100.

Florek, C. A. & Tucker, C. L. 2005 Stretching distributions in chaotic mixing of droplet dispersions with unequal viscosities. *Phys. Fluids* **17**, 053101.

Franjione, J. G. & Ottino, J. M. 1992 Symmetry concepts for the geometric analysis of mixing flows. *Philos. Trans. R. Soc. Lond.* A **338**, 301–323.

Froyland, G. & Padberg, K. 2009 Almost-invariant sets and invariant manifolds: connecting probabilistic and geometric descriptions of coherent structures in flows. *Physica* D **238**, 1507–1523.

Gibout, S., Guer, Y. L. & Schall, E. 2006 Coupling of a mapping method and a genetic algorithm to optimize mixing efficiency in periodic chaotic flows. *Commun. Nonlinear Sci. Numer. Simul.* **11**, 413–423.

Giona, M., Adrover, A., Cerbelli, S. & Vitacolonna, V. 2004 Spectral properties and transport mechanisms of partially chaotic bounded flows in the presence of diffusion. *Phys. Rev. Lett.* **92**, 114101.

Giona, M., Cerbelli, S. & Adrover, A. 2002 Geometry of reaction interfaces in chaotic flows. *Phys. Rev. Lett.* **88**, 024501.

Gleeson, J. P. 2005 Transient micromixing: examples of laminar and chaotic stirring. *Phys. Fluids* **17**, 100614.

Gouillart, E., Thiffeault, J.-L. & Finn, M. D. 2006 Topological mixing with ghost rods. *Phys. Rev.* E **73**, 036311.

Gubanov, O. & Cortelezzi, L. 2009 Sensitivity of mixing optimization to the geometry of the initial scalar field. In *Analysis and Control of Mixing with an Application to Micro and Macro Flow Processes* (ed. L. Cortelezzi & I. Mezić), *CISM Courses and Lectures* 510, pp. 369–405. Springer.

Hobbs, D. M., Alvarez, M. M. & Muzzio, F. J. 1997 Mixing in globally chaotic flows: a self-similar process. *Fractals* **5**, 395–425.

Hobbs, D. M. & Muzzio, F. J. 1997 Effects of injection location, flow ratio and geometry on kenics mixer performance. *Am. Inst. Chem. Eng. J.* **43**, 3121–3132.

Kolda, T. G. 2005 Revisiting asynchronous parallel pattern search for nonlinear optimization. *SIAM J. Optimization* **16** (2), 563–586.

Lawler, E. L. & Wood, D. E. 1966 Branch-and-bound methods: a survey. *Operations Res.* **14**, 699–719.

Lewis, R. M. & Torczon, V. 2000 Pattern search methods for linearly constrained minimization. *SIAM J. Optimization* **10**, 917–941.

Liu, M., Muzzio, F. J. & Peskin, R. L. 1994 Quantification of mixing in aperiodic chaotic flows. *Chaos Solitons Fractals* **4**, 869–893.

Malvern, L. E. 1969 *Introduction to the Mechanics of a Continuous Medium*. Prentice-Hall.

Mathew, G., Mezić, I., Grivopoulos, S., Vaidya, U. & Petzold, L. 2007 Optimal control of mixing in stokes fluid flows. *J. Fluid Mech.* **580**, 261–281.

Mathew, G., Mezić, I. & Petzold, L. 2005 A multiscale measure for mixing and its applications. *Physica* D **211**, 23–46.

Muzzio, F. J., Alvarez, M. M., Cerbelli, S., Giona, M. & Adrover, A. 2000 The intermaterial area density generated by time- and spatially periodic 2d chaotic flows. *Chem. Engng Sci.* **55**, 1497–1508.

O'Naraigh, L. & Thiffeault, J.-L. 2008 Bounds on the mixing enhancement for a stirred binary fluid. *Physica* D **237**, 2673–2684.

Ottino, J. M. 1989 *The Kinematics of Mixing: Stretching, Chaos, and Transport*. Cambridge University Press.

Paul, E. L., Atiemo-Obeng, V. A. & Kresta, S. M. (Ed.) 2004 *Handbook of Industrial Mixing: Science and Practice*. Wiley.

Phelps, J. H. & Tucker, C. L. 2006 Lagrangian particle calculations of distributive mixing: limitations and applications. *Chem. Engng Sci.* **61**, 6826–6836.

Pierrehumbert, R. T. 1994 Tracer microstructure in the large-eddy dominated regime. *Chaos Solitons Fractals* **4**, 1091–1110.

Pierrehumbert, R. T. 2000 Lattice models of advection-diffusion. *Chaos Solitons Fractals* **10**, 61–74.

Rodrigo, A. J. S., Mota, J. P. B., Lefevre, A. & Saatdjian, E. 2003 On the optimization of mixing protocol in a certain class of three-dimensional stokes flows. *Phys. Fluids* **15**, 1505–1516.

Shaw, T. A., Thiffeault, J.-L. & Doering, C. R. 2007 Stirring up trouble: multi-scale mixing measures for steady scalar sources. *Physica* D **231**, 143–164.

Singh, M. K., Anderson, P. D., Speetjens, M. F. M. & Meijer, H. E. H. 2008*a* Optimizing the rotated arc mixer. *Am. Inst. Chem. Eng. J.* **54**, 2809–2822.

Singh, M. K., Kang, T. G., Meijer, H. E. H. & Anderson, P. D. 2008*b* The mapping method as a toolbox to analyse, design, and optimize micromixers. *Microfluid Nanofluid* **5**, 313–325.

Stremler, M. A. 2009 Fluid mixing, chaotic advection, and microarray analysis. In *Analysis and Control of Mixing with an Application to Micro and Macro Flow Processes* (ed. L. Cortelezzi & I. Mezić), *CISM Courses and Lectures* 510, pp. 323–337. Springer.

Stremler, M. A. & Cola, B. A. 2006 A maximum entropy approach to optimal mixing in a pulsed source-sink flow. *Phys. Fluids* **18**, 011701.

Sturman, R., Ottino, J. M. & Wiggins, S. 2006 *The Mathematical Foundations of Mixing: The Linked Twist Map as a Paradigm in Applications: Micro to Macro, Fluids to Solids*. Cambridge University Press.

Szalai, E. S., Kukura, J., Arratia, P. E. & Muzzio, F. J. 2003 Effect of hydrodynamics on reactive mixing in laminar flows. *Am. Inst. Chem. Eng. J.* **49**, 168–179.

Szalai, E. S. & Muzzio, F. J. 2003 Fundamental approach to the design and optimization of static mixers. *Am. Inst. Chem. Eng. J.* **49**, 2687–2699.

Thiffeault, J.-L., Doering, C. R. & Gibbon, J. D. 2004 A bound on mixing efficiency for the advection-diffusion equation. *J. Fluid Mech.* **521**, 105–114.

Thiffeault, J.-L. & Pavliotis, G. A. 2008 Optimizing the source distribution in fluid mixing. *Physica* D **237**, 918–929.

Vikhansky, A. & Cox, S. M. 2007 Conditional moment closure for chemical reactions in laminar chaotic flows. *Am. Inst. Chem. Eng. J.* **53**, 19–27.

Zalc, J. M. & Muzzio, F. J. 1999 Parallel–competitive reactions in a two-dimensional chaotic flow. *Chem. Engng Sci.* **54**, 1053–1069.

Zalc, J. M., Szalai, E. S. & Muzzio, F. J. 2003 Mixing dynamics in the SMX static mixer as a function of injection location and flow ratio. *Polym. Engng Sci.* **43**, 875–890.